Defence Science Journal, Vol. 64, No. 5, September 2014, pp.417-425, DOI : 10.14429/dsj.64.5191

Numerical Investigation of Hydrogen-fuelled Scramjet Combustor with Cavity Flame Holder

Malsur Dharavath, P. Manna, and Debasis Chakraborty*

Defence Research and Development Laboratory, Hyderabad-500 258, India
**E-mail: debasis_cfd@drdl.drdo.in*

ABSTRACT

Reacting flow field of a cavity-based hydrogen-fuelled supersonic combustion ramjet (scramjet) combustor has been explored numerically. 3-D RANS equations are solved alongwith k-ε turbulence model and infinitely fast rate kinetics for combustion. The flow field inside the flame holding cavity and its effect on the mixing and reaction are explored in detail by performing simulations of two different combustors (with and without cavities) for which elaborate surface pressure measurements are available for reacting and non-reacting flows. Simulations capture all the finer details of the flow field and good match between computed surface pressures experimental values for different equivalence ratios forms the basis of further analysis. The cavity of the combustor behaves as an open cavity for both non-reacting and reacting flow-even though the flow patterns inside the cavity are quite different for both the cases. Flame-holding cavities are seen to augment mixing and reaction in small sized combustors.

Keywords: Supersonic combustion ramjet, scramjet combustor, cavity flame holder

1. INTRODUCTION

Sustained flight at hypersonic speed in the atmosphere remains the largest unexplored region of the possible flight envelope. Development of air-breathing hypersonic technology has been the subject of renewed interest since 1980s because of tremendous military and commercial opportunities. The success of efficient design of such a trans-atmospheric hypersonic vehicle depends largely on the proper choice of the propulsion system, which is capable of producing large thrust to overcome the drag experienced by the vehicle. These types of vehicles, according to current proposals, use supersonic combustion ramjet (scramjet) propulsion system. The research and development of scramjet engine technologies carried out in various countries like USA, Russia, France, Japan, Germany, Australia, and other countries for last four decades has been reviewed by Curran[1]. Two emerging applications, namely hydrogen- and hydrocarbon-fuelled engines are mainly emphasised for the use in space and military purposes respectively.

A detailed understanding of the complex mixing and combustion process inside the combustor is required for the development of efficient scramjet engines. The flow field inside the scramjet combustor is fully three-dimensional with strong shock boundary layer interaction, which causes flow separation. Fluid dynamics and chemistry interact very strongly inside the scramjet combustor. Detailed flow investigations have been performed in various countries on different aspects of scramjet flow field including ignition, flame holding, fuel injection and intake combustor interaction for both hydrogen and kerosene fuels. Efforts were made to focus on different injection schemes like cavity, strut, pylon, etc. for different geometrical configurations for fuel injection and flame-holding in scramjet combustor. Various methods to enhance the mixing process in the scramjet engines are reported[2]. Some of the passive mixing devices like ramps, tabs, lobe mixers, vanes, backward facing step, port, cavity, etc. use streamwise vorticity, swirl, and acoustic excitation; while the active devices like vibrating splitter, pulsed jet, Helmholtz resonator, and piezoelectric actuators use forced excitation to augment mixing. Cavity flame holders were found to facilitate self-ignition and flame stabilisation due to substantial reduction of the critical equivalence ratio for stable combustion with the use of cavities. The physical mechanisms involved in cavity-based flame holder on supersonic combustor are quiet complex and not properly understood. The existing definitions of open- and closed-cavity characteristics are based on non-reacting flows and are subject to revision for reacting flow situations. It is generally recognised that open cavities ($L/h < 10$) could be used for flame-holding while the mixing enhancement could be achieved through the closed cavities. An overview of the research efforts using cavity as flame holder and flame stabilisation with its effectiveness in scramjet flow field has been presented in details[3]. Yu[4], *et al.* investigated experimentally eight different types of integrated wall injector cavity configurations to study the flame holding characteristics and combustor performance in scramjet combustor using hydrogen fuel. Both experimental and computational investigations[5-8] were carried out to study the flame characteristics and flame stabilisation and combustion enhancement using cavity as a flame holder. Effects of cavity length, depth, aft ramp angle, backpressure, etc on flow characteristics were studied in detail. Huang[7], *et al.* studied numerically the effect of cavity length-to-depth ratio

Received 12 November 2013, Revised 25 August 2014, online published 22 September 2014

(*L/h*) and backpressure on the scramjet combustor flow field for non-reacting flow. Numerical investigation of combustion enhancement using cavity flame holder has been studied by Kim[8], *et al.* to determine the effects of cavity length, depth, aft wall angle on combustion efficiency and total pressure loss.

Advanced flow models (including RANS, LES) and chemical kinetics involving multispecies and multi reaction paths were studied extensively in the literature to simulate supersonic combustion with hydrogen fuel. Recently, Murty and Chakraborty[9] have demonstrated that standard engineering tools (simple chemical kinetic scheme and simple combustion model) can predict overall features of the mixing and reaction in a hydrogen-fuelled scramjet combustor. From literature it is observed that many conclusions arrived for cavity performance are derived from the non-reacting flow. But, for reacting flows, caused due to wall injection, the flow properties are altered significantly ahead and inside the cavity. So the high-speed reacting flow past cavities requires further study. In the present work, the experimental conditions of cavity-based scramjet combustor with hydrogen fuel[4] are explored numerically. Three-dimensional Reynolds Averaged Navier–Stokes (RANS) equations, along with standard k–ε turbulence model[10], species transport equations and the eddy-dissipation reaction models have been solved to investigate the flow field numerically using commercial CFD software[11]. The computed results are compared with the surface pressures reported in the literature[4] and good comparison of experimental wall pressure with computational values forms the basis of in-depth analysis of cavity characteristics in the present study. Thermochemical parameters in the combustor have been analysed to understand the cavity characteristics in high-speed reacting flow.

2. EXPERIMENTAL SET-UP FOR CARRYING OUT COMPUTATIONS

The schematic of cavity-based scramjet combustor experiment[4] for which the computations are carried out is shown in Fig. 1. Eight different types of integrated wall injector cavity configurations were designed and tested at various stagnation conditions with hydrogen fuel. High temperature vitiated air was produced by burning of hydrogen, oxygen, and air in a heater, keeping the volume fraction equal to that of THE normal air. For all cases, the nominal Mach number at the entrance of the combustor entrance was 2.5, which was produced by the expansion of hot vitiated air through a two-dimensional nozzle attached to with the heater. Although the experimental condition of Yu[4], *et al.* considered eight different combustor configurations; the present study has considered two combustor geometries, with and without cavities, to investigate the detailed flow features inside the cavity. Detailed descriptions of the experiments are available in Yu[4], *et al.* Combustor geometrical dimensions and inflow parameters are shown in Table 1. Combustor 1 has no cavity while the combustor 2 has a cavity of with $L/h = 3.0$ with ramp aft angle 45°. Stagnation pressure and temperature for both the combustors are 1.3 MPa, and 1900 K, respectively. The combustor is fitted with flush-mounted interchangeable cavity modules on the top and bottom walls of the combustor. Sonic hydrogen gas was injected normally to the vitiated air stream via sixteen orifices (eight from top wall and eight from the bottom wall) of 1.6 mm diameter located at an axial location of 140 mm from combustor inlet. In the present simulation, four different fuel equivalence ratios (0.46, 0.7, 0.93, and 1.14) were considered to understand the flow behaviour in fuel-lean as well as fuel-rich conditions.

Table 1. Geometrical dimension of the combustors and inflow parameters

Combustor details	Combustor 1	Combustor 2
Length (mm)	595	672
Width (mm)	70	70
Section-I length (mm) & divergence (deg)	140 & 1.0	140 & 1.0
Section-II length (mm) & divergence (deg)	155 & 1.0	155 & 5.0
Section-III length (mm) & divergence (deg)	300 & 3.0	377 & 5.0
Cavity length (L, mm) & depth (h, mm)	-----	30 & 10
Cavity location from combustor inlet (mm)	-----	150
Location of fuel injection from combustor inlet (mm)	140	140
Test gas	Vitiated air	
P_o (MPa)	1.3	
T_o (K)	1900	
Fuel	H_2	
Fuel injection Mach no	1.0	
T_o of fuel (K)	295	
Nos. of H_2 injector and diameter (mm)	16 & 1.6	
Fuel equivalence ratio	0.46, 0.7, 0.93, 1.14	0.7

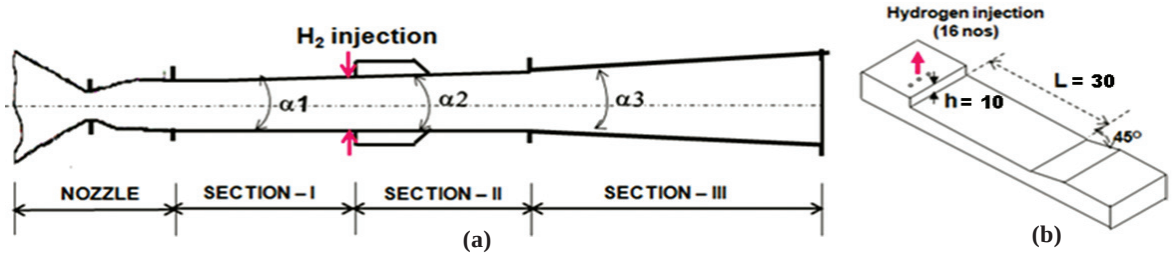

Figure 1. Experimental set-up[4] for carrying out computations : (a) combustor and, (b) cavity module.

3. COMPUTATIONAL METHODOLOGY

Three-dimensional Reynolds Averaged Navier Stokes (RANS) equations were solved using CFX-code[3], which is an integrated software system capable of solving diverse and complex multidimensional fluid flow problems. The code is fully implicit, finite volume method with finite element-based discretization of geometry. The convective terms are discretized through 2nd order scheme and k - ε turbulence model with wall function was used. Hydrogen-air reaction is represented on a molar basis by $2H_2+O_2=2H_2O$ and the eddy dissipation combustion model was used. Log-normalised maximum residue of -04 was considered as the convergence criteria. The details of the governing equations, thermodynamics and the discretization schemes are given in the following subsections. To find out the accuracy and the range of applications, the software has been validated for various reacting and non-reacting flows pertaining to the scramjet combustor including transverse sonic injection in a supersonic flow[12], transverse H_2 injection in constant area duct[13], H_2 injection from struts[14,15] and pylon injectors[16]. All these validation exercises have revealed that although the computed pressures overpredict the experimental values in the injection zone, the computational and experimental values of the flow parameters match fairly well in the divergent portion of the combustor where the major portion of thrust is produced.

3.1 Governing Equations

The system of equations governing the conservation of mass, momentum, energy, and species conservation of a multispecies, turbulent , compressible gas has been derived in Williams[17]. These equations are expressed as:

Continuity equation**:**

$$\frac{\partial \rho}{\partial t}+\frac{\partial}{\partial x_k}(\rho u_k)=0 \qquad k=1,2,3$$

Momentum equation **:**

$$\frac{\partial}{\partial t}(\rho u_i)+\frac{\partial}{\partial x_k}(\rho\, u_i\, u_k)+\frac{\partial P}{\partial x_i}=\frac{\partial(\tau_{ik})}{\partial x_k},\ i,\ k=1,2,3$$

Energy equation **:**

$$\frac{\partial}{\partial t}(\rho\, H)+\frac{\partial}{\partial x_k}(\rho\, u_k H)=-\frac{\partial}{\partial x_k}(u_j\,\tau_{jk})+\frac{\partial q_k}{\partial x_k},\ j,\ k=1,2,3$$

Turbulent kinetic energy (K) equation :

$$\frac{\partial}{\partial t}(\rho K)+\frac{\partial}{\partial x_k}(\rho u_k K)=\frac{\partial}{\partial x_k}\left(\left(\frac{\mu_l}{\mathrm{Pr}}+\frac{\mu_t}{\sigma_K}\right)\frac{\partial K}{\partial x_k}\right)+S_K$$

Rate of dissipation of turbulent kinetic energy (ε) equation:

$$\frac{\partial}{\partial t}(\rho\varepsilon)+\frac{\partial}{\partial x_k}(\rho u_k\varepsilon)=\frac{\partial}{\partial x_k}\left(\left(\frac{\mu_l}{\mathrm{Pr}}+\frac{\mu_t}{\sigma_\varepsilon}\right)\frac{\partial \varepsilon}{\partial x_k}\right)+S_\varepsilon$$

Species mass fraction (Z) :

$$\frac{\partial}{\partial t}(\rho Z)+\frac{\partial}{\partial x_k}(\rho u_k Z)=\frac{\partial}{\partial x_k}\left(\left(\frac{\mu_l}{\mathrm{Pr}}+\frac{\mu_t}{\sigma_c}\right)\frac{\partial Z}{\partial x_k}\right)$$

where ρ, u_i, p, H are the density, velocity components, pressure and total enthalpy, respectively and $\mu = \mu_l + \mu_t$ is the total viscosity; μ_l, μ_t being the laminar and turbulent viscosities and Pr is the Prandtl number. The source terms S_k and S_ε of the K and ε equation are defined as

$$S_K=\tau_{ik}\frac{\partial u_i}{\partial x_k}-\rho\varepsilon \quad \text{and} \quad S_\varepsilon=C_{\varepsilon 1}\tau_{ik}\frac{\partial u_i}{\partial x_k}-C_{\varepsilon 2}\frac{\rho\varepsilon^2}{K}$$

where turbulent shear stress is defined as

$$\tau_{ik}=\mu_t\left(\frac{\partial u_i}{\partial x_k}+\frac{\partial u_k}{\partial x_i}\right)$$

Laminar viscosity (μ_l) is calculated from Sutherland law as

$$\mu_l=\mu_{ref}\left(\frac{T}{T_{ref}}\right)^{3/2}\left(\frac{T_{ref}+S}{T+S}\right)$$

where T is the temperature and μ_{ref}, T_{ref} and S are known coefficients. The turbulent viscosity μ_t is calculated as

$$\mu_t=c_\mu\frac{\rho K^2}{\varepsilon}$$

The coefficients involved in the calculation of μ_t are taken as

c_μ =0.09, $C_{\varepsilon 1}$=1.44, $C_{\varepsilon 2}$ = 0.92
σ_K =1.0, σ_ε =1.3, σ_c = 0.9

The heat flux q_k is calculated as $q_k=-\lambda\frac{\partial T}{\partial x_k}$, λ is the thermal conductivity.

3.2 Thermodynamics Model

A thermally perfect gas is assumed in the present study and, consequently, the specific heats for all species are function of temperature only. The specific heats were calculated using a fourth-order polynomial at the internal of fluid temperature 300 K – 5000 K. In each interval, the same form for the polynomials is used but different coefficients can be used.

$$\frac{C_{p_i}}{R}=A_i+B_iT+C_iT^2+D_iT^3+E_iT^4$$

where A_i, B_i, C_i, D_i and E_i are curvefit constants and T is the fluid static temperature. C_{p_i} is linearly extrapolated when the fluid temperature T < 300 K or T > 5000 K. Then, the static enthalpy h, is calculated as $h=\sum_{i=1}^{n}\alpha_i h_i(T)$ and the static enthalpy of each species $h_i(T)$, is $h_i(T)=\Delta h_{fi}^o+\int_{T^o}^{T}C_{p_i}(T)dT$

where Δh_{fi}^o is the standard heat of formation of species I, defined as the heat evolved when one mole of substance is formed from its elements in their respective standard states at 298.15 K and 1.0 atmosphere. The fluid temperature is calculated based on the solution of the fluid enthalpy using a Newton's iteration method for finding the roots of the polynomials. An equation of state of the following form for a multi-component was used to calculate fluid density $\rho = P/(RT/M_w)$, where the mixture molecular weight is obtained by the following equation, $M_w=\left(\sum_{i=1}^{n}(\alpha_i/M_w)\right)^{-1}$ and R is the universal gas constant.

The Gibbs free energy is required to determine the equilibrium constants for the combined eddy dissipation and finite rate chemistry models. It was obtained for a constant pressure process by

$$\frac{g_i}{R}=A_i(T-\ln T)-\frac{B_i}{2}T^2-\frac{C_i}{6}T^3-\frac{D_i}{12}T^4-\frac{E_i}{20}T^5+F_i-G_iT$$

where G_i is an additional curvefit constant.

3.3 Combustion Modelling

The single-step global kinetics scheme was adopted in light of its simplicity and reasonably accurate modelling of the burned gas containing completely oxidised species of hydrogen (H_2) fuel. The scheme for H_2 - oxidation involves the following one step (global step) reaction and three species:

$2H_2 + O_2 \rightarrow 2H_2O$

The effect of turbulent mixing on combustion has been taken into account by means of the eddy-dissipation model (EDM). In this model, the chemical reaction is fast relative to the transport process in the flow. When, reactants mix at the molecular level these instantaneously form products. The model assumes that the reaction rate may be related directly to the time required to mix reactants at the molecular level. In turbulent flows, this mixing time is dictated by the eddy properties, and therefore, the burning rate is proportional to the rate at which turbulent kinetic energy is dissipated, i.e., reaction rate $\alpha\ \varepsilon/k$, where k is the turbulent kinetic energy and ε is its rate of dissipation. The reaction rate associated with turbulent mixing, is given by the minimum of the following three rates.

$$R_{H_2,edm} = A_{ed}\rho\frac{\varepsilon}{k}\min\left\{Y_f, \frac{Y_o}{\nu_{H_2}}, B_{ed}\frac{Y_p}{1+\nu_{H_2}}\right\}$$

where, Y_f , Y_o and Y_p are the mass fraction of fuel, oxidant and products respectively, A_{ed} and B_{ed} are empirical constants taken to be 4.0 and 0.5, respectively, ν_{H_2} is stoichiometric coefficients of H_2 reaction.

3.4 Discretisation of Governing Equations

The CFX-11 solver utilises a finite volume approach, in which the conservation equations in differential form are integrated over a control volume described around a node, to obtain an integral equation. The pressure integral terms in the momentum integral equation and the spatial derivative terms in the integral equations are evaluated using finite element approach. An element is described with eight neighbouring nodes. The advective term is evaluated using upwind differencing with physical advection correction. The set of discretised equations form a set of algebraic equations: $A\vec{x} = b$ where, $\vec{x}$ is the solution vector. The solver uses an iterative procedure to update an approximated x_n (solution of x at n^{th} time level) by solving for an approximate correction x' from the equation $A\vec{x}' = \vec{R}$, where $\vec{R} = \vec{b} - A\vec{x}_n$ is the residual at n^{th} time level. The equation $A\vec{x}' = \vec{R}$ is solved approximately using an approach called Incomplete Lower Upper factorisation method. An algebraic multigrid method is implemented to reduce low frequency errors in the solution of the algebraic equations. Maximum residual $\left(= \phi_j^{n+1} - f\left(\phi_j^{n+1}, \phi_j^n\right)\right) < 10^{-4}$ is taken as convergence criterion.

4. RESULTS AND DISCUSSION

4.1 Grid Generation and Boundary Conditions

Taking the advantage of symmetry in the geometry, only one-fourth geometry of the combustor has been considered for the simulation. Multi-block structured grid with 1.1 million cells (450×45×55) are generated for 1/4th geometry. Typical grid structure for the combustor-2 along with the blown-up view near the cavity is shown in Fig. 2.

The grids are much clustered near the inflow plane, solid walls, and cavity region to capture the finer details of the flow. The origin of the computational domain has been taken at the middle of the combustor entry. In the simulation, X-axis was taken along the length of the combustor while Y and Z axes were taken along the height and width of the combustor respectively. The facility nozzle from the throat onwards was considered along with the combustor to get a realistic boundary layer profile at the inlet of the combustor. The sonic condition, no-slip and adiabatic wall and supersonic outflow conditions are prescribed in fuel inflow, wall and outflow boundaries, respectively. The average Mach number at the combustor inlet has been found to be about 2.5 which agrees well with the experimental observations.

4.2 Combustor-1 Flow Characteristics

Mach number distributions for non-reacting and reacting flows for equivalence ratio (φ) 0.46 in the symmetry plane for combustor-1 are shown in Fig. 3. Predominant supersonic flow was observed in non-reacting flow throughout the combustor. Mach numbers were well above unity everywhere inside the combustor. However, for the reacting case, fuel injection and reaction caused the occurrence of complex shock reflections inside the combustor. The upstream interactions became more intense with increase in equivalence ratio. To quantify the effect, simulations were carried out for different equivalence ratios and the upstream interaction distance is plotted with fuel equivalence ratio in Fig. 4.

Flow upstream interaction location is defined as the axial distance from the combustor inlet where predominant supersonic flow becomes subsonic in the core region of flow, as shown in Fig. 3. With the injection of more fuel, i.e., increase of equivalence ratio, the upstream interaction increases and

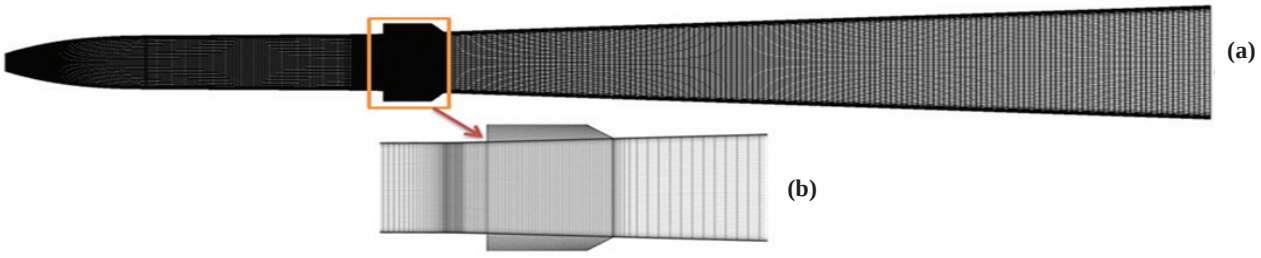

Figure 2. Computational grid : (a) Combustor-2 and (b) Blown-up view near the cavity.

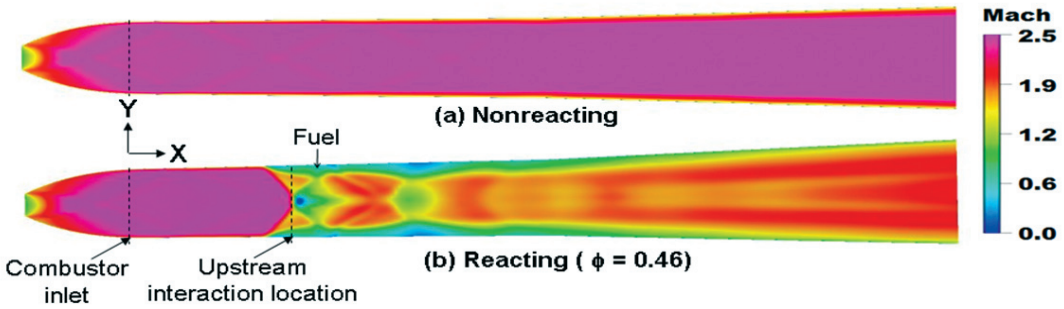

Figure 3. Mach number distribution for Combustor-1.

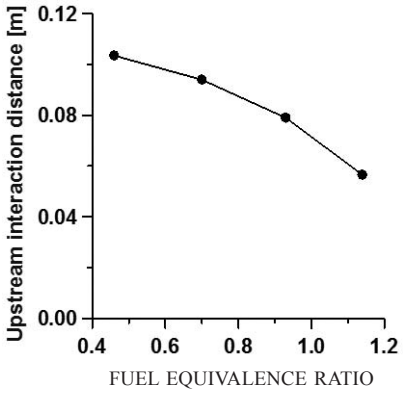

Figure 4. Location of upstream interaction from combustor inlet.

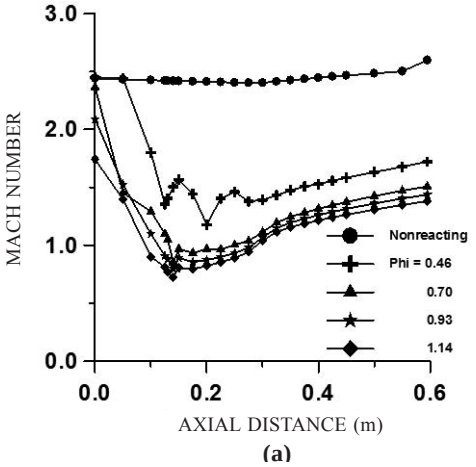

(a)

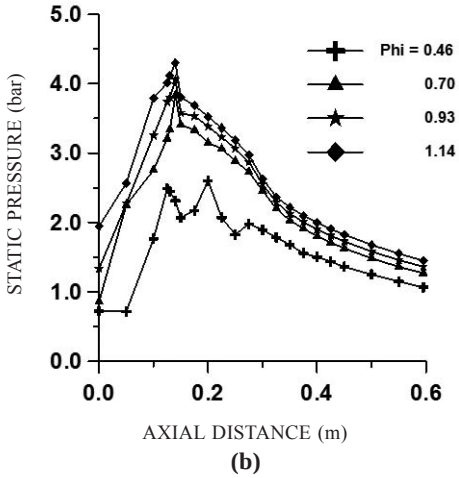

(b)

Figure 5. Comparison of average : (a) Mach number and (b) static pressure for various equivalence ratios.

the interaction locations move towards combustor inlet. This upstream interaction is also responsible for lower Mach number and higher static pressure ahead of the fuel injection (Fig.5). Average Mach number decreased initially and then increased in the divergent portion of the combustor in reacting flow (Fig.5(a)). The average Mach number along the length of the combustor was found above unity even though subsonic pockets in the reaction zones have been observed for φ=0.46 (Fig.5(b)). However, for other equivalence ratios (φ =0.70, 0.93, 1.14), the average Mach number has been found to be subsonic in the reactive-intense zones. The exit Mach number decreased with the increase of equivalence ratio. The exit Mach numbers were 1.72, 1.51, 1.44, and 1.38 for at φ =0.46, 0.70, 0.93, and 1.14, respectively. Comparisons of top wall pressure between experimental and computation are shown in Fig. 6. Computed top wall pressures match extremely well with the experimental results for non-reacting flow (φ=0.0). For reacting flow case, in the fuel injection zone, computation over-predicts the surface pressures because of the fast chemistry assumption in the simulation. But in the divergent section of the combustor, where most of the thrust is produced, the computed values agree well with the experimental values for all the equivalence ratios studied.

4.3 Combustor-2 Flow Field and Cavity Characteristics

Mach number distributions in the symmetry plane for combustor-2 are shown in Fig. 7 both for non-reacting and

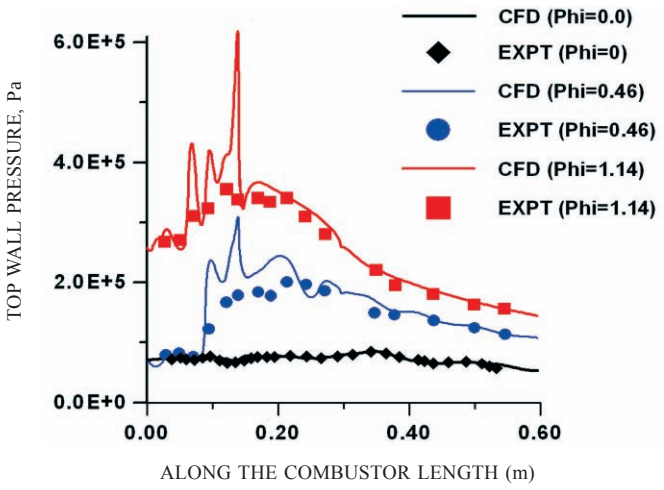

Figure 6. Comparison of wall pressures between experiment and computation.

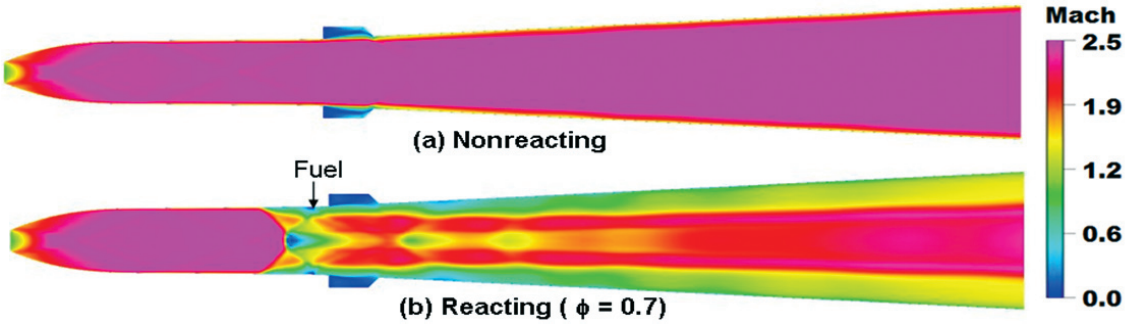

Figure 7. Mach number distribution for Combustor-2.

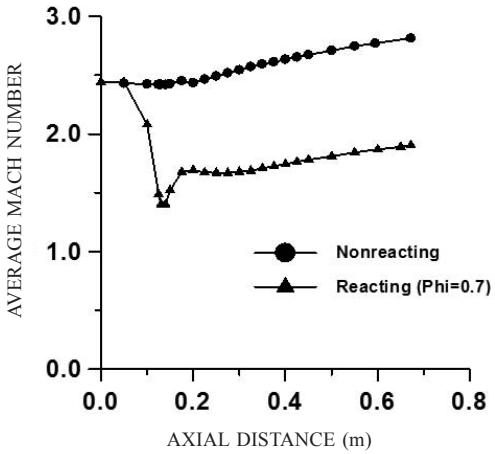

Figure 8. Comparison of average Mach number between non-reacting and reacting flows.

reacting flows (φ =0.7). The upstream interaction location has been found to be X=0.1182 m from combustor entry. Reacting flow average Mach number sharply decreased due to the reaction of fuel adjacent to the cavity regions (Fig. 8). However, the average Mach number was above unity everywhere along the length of the combustor. The exit Mach numbers were 2.82 and 1.90 for non-reacting and reacting flows, respectively.

The flow field inside the cavity has been studied in detail. Velocity vectors near the cavity region for reacting and non-reacting cases are shown in Fig. 9. In both the cases, the core flow was not seen to impinge inside the cavity. The velocity above the cavity was almost the same as free stream velocity about 1600 m/s in non-reacting flow, whereas, the same was decreased to about 1200 m/s for reacting flow due to the fuel injection and the combustion of fuel. Recirculating flow pattern within the cavity was found to be quiet different between reacting and non-reacting flows. A well-defined re-circulating bubble was seen in the cavity for non-reacting flow; whereas,

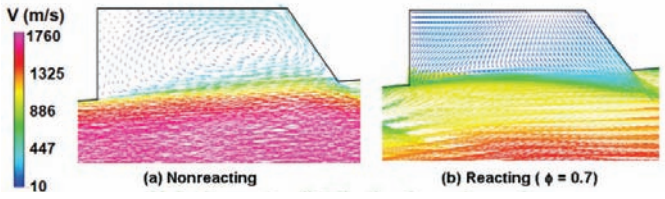

Figure 9. Velocity vector plot in cavity region (combustor-2).

two weak re-circulation bubbles were seen in the cavity for reacting flow case. Although, the flow pattern inside the cavity region is markedly different between the reacting and non-reacting flow cases, the present cavity behaving like an open cavity for both the reacting and non-reacting flow cases. It is to be noted that the length-to-depth ratio (*L/D*) of the cavity is only 3.0, which is much below the limiting value of 10.

Reacting flow top wall pressure comparisons between experimental and computation are shown in Fig. 10. Wall pressure increases suddenly due to the injection of the fuel. Higher values of wall pressure have been observed adjacent to the cavity regions due to the reaction of the fuel. Computed top wall pressures match extremely well with the experimental results in the regions before the fuel injection and in the divergent combustor. The upstream interaction caused due to fuel injection is well captured in the simulation. However, in the fuel injection zone, comparatively higher pressures have been observed in CFD compared to the experimental measured values because of the fast chemistry assumption in the simulation as discussed earlier.

4.4 Comparison of Results between Combustor-1 and Combustor-2 for φ= 0.7 – Effect of Cavity

To find the effect of cavity on the flow field, the computed flow field without cavity (Combustor -1) and with cavity (Combustor -2) are compared for the same equivalence ratio 0.7. Figure 11 depicts the comparisons of cross-sectional

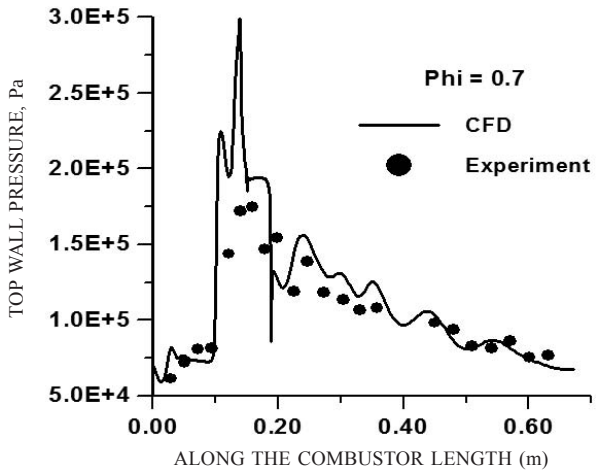

Figure 10. Comparison of wall pressures between experiment and computation.

distribution of Mach numbers at different axial stations [X = 0.0 (combustor entry), 0.1, 0.16, 0.2, 0.3, and 0.5] for the two combustors for φ = 0.7. Computed Mach numbers are found to be less in combustor-1 compared to combustor-2. This is due to more expansion in combustor -2 because of higher divergence (divergence angle was 5° and 3° in combustor -2 compared to 1° and 3° in combustor-1) In fact, the combustor-1 has the sections-1 and 2 to be almost flat (1° divergent) up to L = 0.295 m. Due to this, static pressure and static temperature rise more for combustor-1. The comparisons of average pressure and temperature for both the combustors are shown in Figs 12 and 13, respectively. Sudden rise of pressure for the combustors is found at X=0.14 m due to the fuel injection normal to the flow.

The combustion process inside the combustor is depicted through the water vapour mass fractions distribution at different axial positions for combustor-1 and combustor-2 in Figs 14(a) and 14(b), respectively. Almost no combustion was observed at X=0.1 m for combustor-1 but combustion was visible at the same location for combustor-2 at the corners, which may be due to the presence of cavity and upstream interaction of the flow. Combustion has been found in the whole cavity region (X=0.16 m) of combustor-2. However, as it proceeds downstream, more zones are covered under combustion in combustor-1 compared to combustor-2. This may be due to the higher upstream pressure and temperature and lesser expansion of the flow geometry.

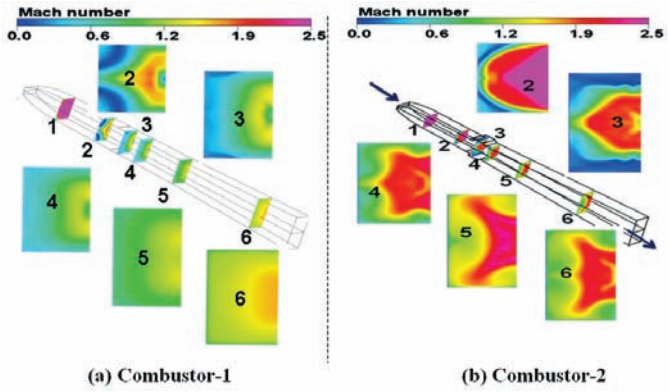

Figure 11. Comparison of Mach number distribution at different axial planes (X = 0 m, 0.1 m, 0.16 m, 0.2 m, 0.3 m, and 0.5 m).

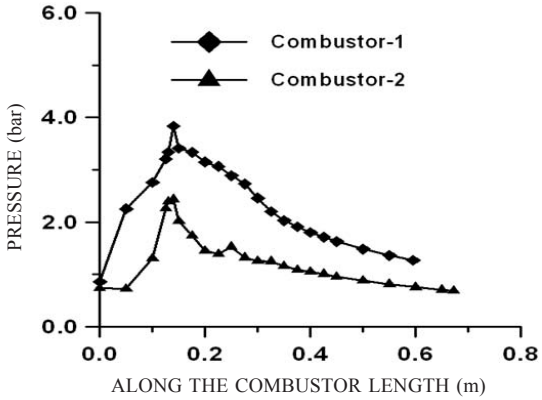

Figure 12. Average static pressure comparison.

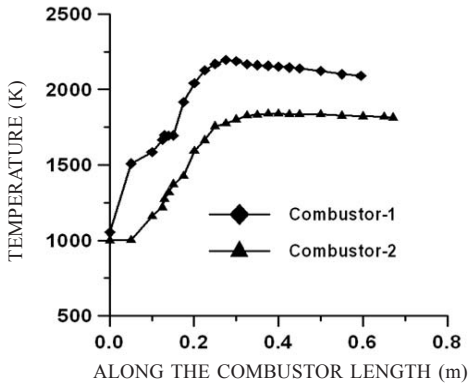

Figure 13. Average static temperature comparison.

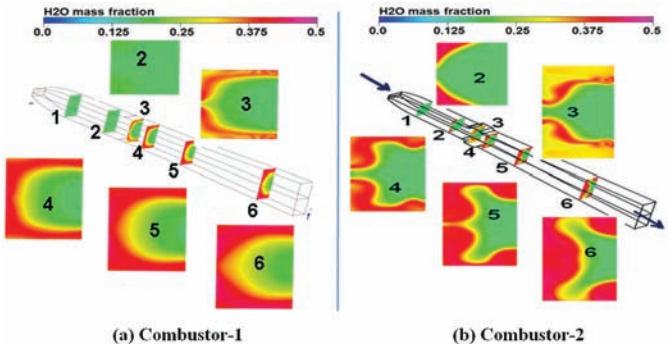

Figure 14. Comparison of H_2O mass fraction at different axial planes (X = 0 m, 0.1 m, 0.16 m, 0.2 m, 0.3 m, and 0.5 m).

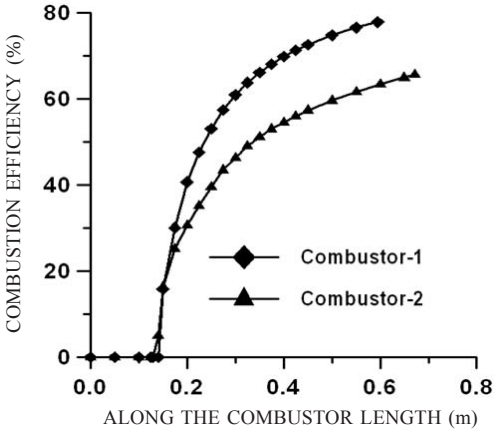

Figure 15. Combustion efficiency comparison.

The amount of fuel burnt has been calculated along the axial length and divided by the amount of total fuel injection to get the combustion efficiency. It has been found that the amount of fuel burnt is more in combustor-1 than combustor-2 which gives better combustion efficiency in combustor-1 as shown in Fig. 15. Due to this, average static pressure and temperature are found to increase more in combustor-1 towards the downstream of the fuel injection (as shown in Figs 12 and 13).

Comparison of availability of thrust has been plotted in Fig. 16. Thrust at any axial location is calculated by equating the momentum of that axial plane and then by subtracting the momentum at the combustor entry. Even though combustor-1 shows higher combustion efficiency, combustor-2 shows

more thrust production which may be due to the higher flow expansion compared to combustor-1. The specific impulse is calculated by dividing the thrust by fuel flow rate and is found to be 979 s and 1233 s for combustor-1 and combustor-2 respectively.

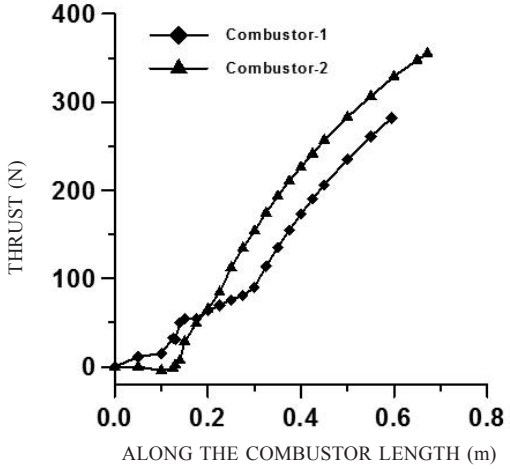

Figure 16. Comparison of thrust along the length.

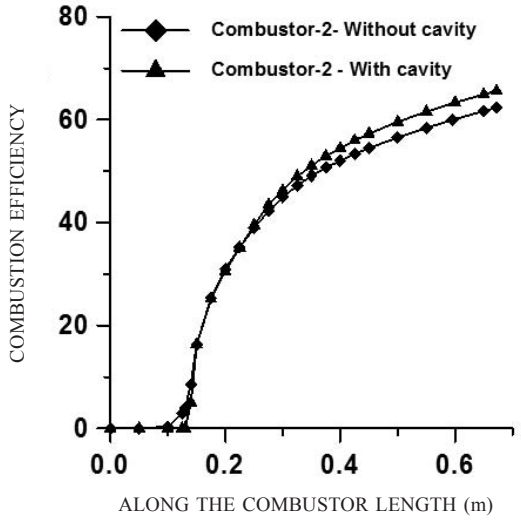

Figure 17. Combustion efficiency comparison.

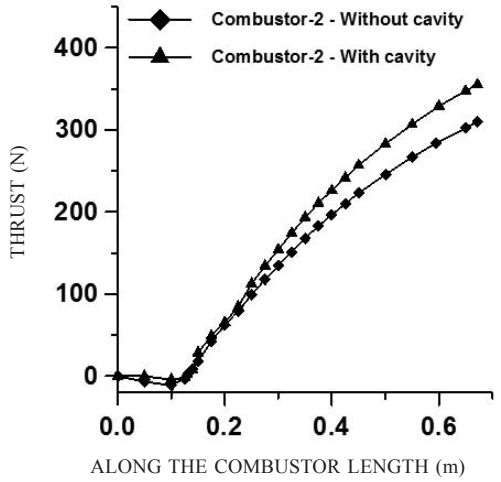

Figure 18. Comparison of thrust along the length.

To compare the performance of the same geometrical configuration, a new simulation was carried out considering the combustor-2 configuration without cavity. The combustor outer envelope, inflow boundary conditions, and the fuel injection remained the same except the deletion of the cavity from combutor-2 geometry. The results of the combustion efficiency and thrust availability are compared in Figs 17 and 18.

The upstream interaction has been found more in the case of without cavity (X= 0.1178 m) compared to with cavity case (X=0.1182 m). Hence, combustion has been found to occur early in the case of without cavity, combustor as shown in Fig. 17. However, more combustion has been found downstream of the cavity (with cavity case) which may be due to better mixing and reaction in presence of cavity. Because of this, higher combustion efficiency has been found at the exit of the combustor in with cavity case (65.6%) compared to without cavity case (62.3%). As a result, almost 14.63% more thrust has been achieved with cavity case compared to without cavity case, as shown in Fig. 18. Small lab-level combustors like the present configuration, cavity can be used effectively for better mixing and combustion and thrust availability in accordance to the flame holding, but the cavity effectiveness needs to be studied for the flight-sized combustor before employing these in the design.

5. CONCLUSIONS

A cavity-based hydrogen-fuelled scramjet combustor is numerically explored for different equivalence ratios. Three-dimensional Navier Stokes equations alongwith k-ε turbulence model and fast chemistry based combustion model are discretised using commercial CFD software. Effect of cavity on mixing and reaction in the combustor is quantified by comparing the results of the combustors with and without cavity. Simulations capture of all the essential features of the mixing and reaction in the scramjet combustor. Computed surface pressures match well with experimental data for different equivalence ratios; although, the computation overpredicts the surface pressure in the fuel injection zone because of fast chemistry assumption. The comparison of cavity flow field between non-reacting and reacting cases reveals that cavity is behaving as open type for both the cases even though the flow patterns in the cavity are markedly different. The cavity can be effectively used for mixing augmentation and combustion in small-scale combustors.

REFERENCES

1. Curran, E.T. Scramjet engines: The first forty years. *J. Propul. Power,* 2001, **17**(6), 1138-1148. doi: 10.2514/2.5875
2. Seiner, John M.; Dash, S.M. & Kenzakowski, D.C. Historical survey on enhanced mixing in scramjet engines. *J. Propul. Power,* 2001, **17**(6), 1273-1286. doi: 10.2514/2.5876
3. Ben-Yakar, Adela & Hanson, Ronald K. Cavity flame-holders for ignition and flame stabilization in scramjets: An overview. *AIAA J. Propul. Power,* 2001, **17**(4), 869-877. doi: 10.2514/2.5818

4. Yu, G.; Li, J.G.; Zhang, X.Y.; Chen, J.H.; Han, B. & Sung, C.J. Experimental investigation on flameholding mechanism and combustion performance in hydrogen-fuelled supersonic combustor. *Combust. Sci. Tech.,* 2002, **174,** 1-27. doi: 10.1080/00102200290021317
5. Sun, M.B.; Wu, H.Y.; Fan, Z.Q.; Wang, H.B.; Bai, X.S.; Wang, Z.G.; Liang, J.H. & Liu, W.D. Flame stabilization in a supersonic combustor with hydrogen injection upstream of cavity flame holders: Experiments and simulations. *Part G: J. Aerosp. Eng.,* 2001, **225,** 1351-1365. doi: 10.1177/0954410011401498
6. Gruber, M.R.; Baurle, R.A.; Mathur, T. & Hsu, K.Y. Fundamental studies of cavity-based flameholder concepts for supersonic combustors. *J. Propul. Power,* 2001, **17**(1),146-153. doi: 10.2514/2.5720
7. Huang, Wei; Wang, Zhen-guo; Yan, Li & Liu, Wei-dong. Numerical validation and parametric investigation on the cold flow field of a typical cavity-based scramjet combustor. *Acta Astrnautica,* 2012, **80**(1),132-140. doi: 10.1016/j.actaastro.2012.06.004
8. Kim, K.M.; Baek, S.W. & Han, C.Y. Numerical study on supersonic combustion with cavity-based fuel injection. *Int. J. Heat Mass Trans.,* 2004, **47,** 271-286. doi: 10.1016/j.ijheatmasstransfer.2003.07.004
9. Murty, M.S.R Chandra & Chakraborty, D. Numerical simulation of angular injection of hydrogen fuel in scramjet combustor. *J. Aerosp. Eng.,* 2012, **226**(7), 861-872. doi: 10.1177/0954410011414320
10. Launder, B.E. & Spalding, D.B. The numerical computation of turbulent flows. *Comput. Methods Appl. Mech. Eng.,* 1974, **3**(2), 269-289. doi: 10.1016/0045-7825(74)90029-2
11. ANSYS CFX, Release 11.0: Installation and Overview, July 2007.
12. Manna, P. & Chakraborty, D. Numerical investigation of transverse sonic injection in a non-reacting supersonic combustor. Proceeding IMechE Part G: *J. Aerosp. Eng.,* 2005, **219,** 205-215. doi: 10.1243/095441005x30261
13. Manna, P. & Chakraborty, D. Numerical simulation of transverse H_2 combustion in supersonic airstream in a constant area duct. *J. Inst. Eng.* (*India*), 2005 86, 47-53.
14. Dharavath, Malsur; Manna, P. & Chakraborty, D. Thermochemical exploration of hydrogen combustion in generic scramjet combustor. *Aerosp. Sci. Tech.,* 2013, **24,** 264-274. doi: 10.1016/j.ast.2011.11.014
15. Saha, S. & Chakraborty, D. Reacting flow computation of staged supersonic combustor with strut injection. *AIAA Paper,* 2006, **3895**.
16. Javed, A. & Chakraborty, D. Numerical simulation of supersonic combustion of pylon injected hydrogen fuel in scramjet combustor. *J. Inst. Eng.* (*India*), 2006, **87**, 1-6.
17. Williams, F. A., Combustion theory, The Benjamin/ Cummings Publishing Company. Menlo park, CA, 1985.

CONTRIBUTORS

Mr Malsur Dharavath obtained his ME (Aerospace Engineering) from Indian Institute of Science (IISc), Bengaluru and is working as a Scientist at the Defence Research and Development Laboratory (DRDL), Hyderabad. He has about 8 journal papers and 9 conference papers to his credit. His research areas include : High-speed reacting and non-reacting flows in missile propulsion including tip-to-tail simulation of hypersonic airbreathing cruise vehicle, scramjet propulsion system, combustion modelling, free-and confined -supersonic jets.

Dr P Manna obtained his PhD (Thermal Science and Engineering) from IIT, Kharagpur. Presently he is working as a Scientist in the Directorate of Computational Dynamics, DRDL, Hyderabad. He has published 12 papers and 20 conference publications in the national and international journalsl. His research interests include: CFD, propulsion, heat transfer, and high-speed reacting flow.

Dr Debasis Chakraborty obtained his PhD (Aerospace Engineering) from Indian Institute of Science (IISc), Bengaluru. Presently, he is working as Technology Director, Computational Dynamics (DOCD), DRDL, Hyderabad. He was the Guest Editor of special issue of Defence Science Journal on CFD. His research areas includes: CFD, aerodynamics, high-speed combustion and propulsion. He has about 140 journal and conference papers to his credit.